Acta Astronautica Vol. 29, No. 1, pp. 1–15, 1993
Printed in Great Britain.

0094-5765/93 $6.00 + 0.00

MINIMUM-FUEL, POWER-LIMITED TRANSFERS BETWEEN COPLANAR ELLIPTICAL ORBITS†

CHRISTINE M. HAISSIG and KENNETH D. MEASE
Department of Mechanical and Aerospace Engineering, Princeton University, Princeton, NJ 08544, U.S.A.
and
NGUYEN X. VINH
Aerospace Engineering Department, University of Michigan, Ann Arbor, MI 48109, U.S.A.

(Received 15 April 1992)

Abstract—Two methods of computing coplanar, minimum-fuel, power-limited transfers are developed, based on approximate solutions obtained by the averaging method. In the first method, the average solution provides estimates of the initial adjoint variables; in the second, it provides approximations of the optimal controls in feedback form. Both trajectory variables and orbit elements are used in developing these methods. Canonical transformations are derived to convert between these sets of coordinates. The accuracy of the methods for computing coplanar, minimum-fuel, power-limited transfers is assessed for a variety of initial and final orbits. Some initial steps are taken toward the characterization of coplanar, minimum-fuel, power-limited transfers for a wide range of thrust to weight ratios. Circle to ellipse and ellipse to ellipse transfers are considered. Details of the trajectories and thrust profiles for a few illustrative cases are presented. These trajectories and thrust profiles are compared to analytical results obtained using the averaging method and to the analytic solution for infinitesimal transfer. The secular behavior of minimum-fuel transfer is predicted by the averaging results. The shape and orientation of the osculating orbits are predicted quantitatively, while the size is predicted qualitatively. The analytic solution for infinitesimal transfer predicts the qualitative behavior of the thrust during each revolution. Some general principles of minimum-fuel, power-limited transfer are revealed.

1. INTRODUCTION

Electric propulsion systems have been under development for many years. Relative to chemical rockets, their major advantage is high specific impulse; their major disadvantage is low thrust capability. Secondary benefits of electric propulsion include precision and variability of thrust levels and specific impulse, generous shutdown and restart capabilities, and the use of chemically passive propellants [1]. Electric propulsion is an attractive type of space propulsion for interplanetary travel and certain Earth orbit missions. Recently it has been proposed for such interplanetary missions as a comet nucleus sample return mission [2], an orbiter mission to Saturn [2], and a mission to a thousand astronomical units [3]. Potential geocentric applications include the transfer of GPS satellites from Shuttle parking orbits to mission orbits [4] and the deployment of a constellation of spacecraft for the Strategic Defense Initiative [5].

For trajectory calculations, a propulsion system is characterized by the available thrust magnitude and direction, the power, and the specific impulse (or ejection velocity). Two idealized propulsion models have most frequently been used [6]. In the constant ejection velocity (CEV) model, either the thrust or thrust acceleration is bounded or thrust impulses are allowed, while the specific impulse is held constant. In the power-limited (LP) model, the power limit, a constant, imposes an upper bound on the product of the thrust magnitude and the specific impulse, which otherwise are free to vary. In both models, the thrust direction is usually unconstrained. Both the CEV and LP models have been employed in the study of minimum-fuel transfer using electric propulsion. The utility of idealized models is that the corresponding minimum-fuel transfer problems are easier to analyze relative to those for more realistic models, and in some cases general results can be obtained. The insight gained from an idealized case provides guidance in tackling more realistic problems and designing specific missions.

For the CEV model, the computation of minimum-fuel transfers in an inverse square gravity field can be reduced to the solution of algebraic equations in the case of impulsive thrust [6,25]. With bounded thrust, asymptotic expansions about the impulsive solution yield good approximations if the thrust is not too low [26,27]. Numerical methods have been used for low thrust levels [28–30]. For the LP model, the minimum-fuel transfer problem is an inverse square field has been solved approximately in the

†Paper IAF-91-346 presented at the *42nd Congress of the International Astronautical Federation*, Montreal, Canada, 7–11 October 1991.

limiting cases of transfer between neighboring elliptic orbits [7,8] and long duration transfer between coplanar elliptic orbits and coaxial orbits [9–11] using linearization and averaging, respectively.

The objective of our research is to develop a comprehensive picture of minimum-fuel, LP transfer. LP results are useful in themselves and are also suggestive of the corresponding CEV results. Our approach is based on the approximate solution to the long duration, minimum-fuel transfer problem obtained by the averaging method [9–11]. In this paper, we limit our attention to the case of transfer between coplanar elliptic orbits. A comprehensive picture of the secular features of long duration, minimum-fuel transfer have been obtained by averaging [9].

We use these results for both qualitative and quantitative guidance in computing and characterizing shorter duration transfers. We show by direct numerical comparison that the average solution remains qualitatively correct for short duration, minimum-fuel LP transfer. Thus, the global understanding of the extremal field obtained from the average solution is not restricted to long duration transfer. Issues of nonuniqueness, local versus global optimality, and conjugate points are clearly resolved for short duration transfers as well.

The average solution also provides a starting point for resolving nonsecular behavior and obtaining quantitatively accurate minimum-fuel transfer solutions. The average solution provides approximations of both the state and costate or adjoint. The average adjoint is used to approximate the minimum-fuel transfer by providing either an approximate minimum-fuel control law or the approximate initial adjoint. A related approach was developed in [12] where an approximate solution for the adjoint, obtained not by averaging but by neglecting the thrust, was used to develop an approximation to the minimum-fuel control law. Numerical integration of the state equations with the approximate control law generates a near minimum-fuel transfer and the associated control history; numerical integration of the state and adjoint equations with the approximate initial adjoint variables generates an extremal transfer that approximately leads to the specified final orbit. The accuracy of the approximate minimum-fuel transfers is assessed by comparison to the exact minimum-fuel transfers. Fuel consumption, terminal conditions, and control histories are compared. The accuracy of the approximate initial adjoint is assessed by looking at the final conditions.

Initial steps toward the characterization of coplanar, minimum-fuel, LP transfers are taken. Transfers from circles to ellipses and ellipses to ellipses for a range of thrust to weight ratios are computed. Details of the trajectories and thrust profiles for a few illustrative cases are presented. The general results for infinitesimal and long duration transfers are used to interpret these results.

2. TRAJECTORY VARIABLE FORMULATION, NECESSARY CONDITIONS, AND FIRST INTEGRALS

Necessary conditions for the solution to the coplanar, minimum-fuel, LP transfer problem have been derived previously by a number of authors [6,9,10,13]. In [13], the equations of motion for the transfer are formulated in terms of the trajectory variables that are used here. The trajectory variables lend themselves to straightforward physical interpretation. In addition, the corresponding equations of motion do not have singularities in the regions of state space of interest and are thus suitable for numerical integration over the entire range of transfers under consideration. The trajectory variables we use are similar to those used in [12]. They are commonly used for atmospheric flight [14,15] and have been used for aeroassisted orbit transfer [16].

The state variables are the radius r, polar angle θ, velocity v, flight path angle γ, and cost J, with the associated adjoint variables p_r, p_θ, p_v, p_γ and p_J. The control variables are the thrust acceleration Γ and the thrust direction δ_t, which is the angle between the velocity vector and the thrust vector. The state and control variables have been nondimensionalized using a reference radius r_{ref} and the reference time $\sqrt{r_{ref}/g_{ref}}$, where g_{ref} is the acceleration of gravity at the reference radius.

Minimizing fuel for a LP transfer is the same as minimizing

$$J = \frac{1}{2}\int_{\tau_0}^{\tau_f} \Gamma^2 \, d\tau, \tag{1}$$

where J is the cost and τ is the nondimensional time [6]. Assuming a central inverse square gravitational field, the equations of motion are

$$\frac{dr}{d\tau} = v \sin\gamma \tag{2}$$

$$\frac{d\theta}{d\tau} = \frac{v\cos\gamma}{r} \tag{3}$$

$$\frac{dv}{d\tau} = -\frac{\sin\gamma}{r^2} + \Gamma\cos\delta_t \tag{4}$$

$$\frac{d\gamma}{d\tau} = \left(\frac{v^2}{r} - \frac{1}{r^2}\right)\frac{\cos\gamma}{v} + \frac{\Gamma\sin\delta_t}{v} \tag{5}$$

$$\frac{dJ}{d\tau} = \tfrac{1}{2}\Gamma^2. \tag{6}$$

The corresponding adjoint equations are

$$\frac{dp_r}{d\tau} = p_\theta\frac{v\cos\gamma}{r^2} - 2p_v\frac{\sin\gamma}{r^3} + p_\gamma\left(\frac{v^2}{r^2} - \frac{2}{r^3}\right)\frac{\cos\gamma}{v} \tag{7}$$

$$\frac{dp_\theta}{d\tau} = 0 \tag{8}$$

$$\frac{dp_v}{d\tau} = -p_r\sin\gamma - p_\theta\frac{\cos\gamma}{r} - p_\gamma\cos\gamma\left(\frac{1}{r} + \frac{1}{v^2r^2}\right) - \frac{p_\gamma^2}{v^3} \tag{9}$$

$$\frac{dp_\gamma}{d\tau} = -p_r v\cos\gamma + p_\theta\frac{v\sin\gamma}{r} + p_v\frac{\cos\gamma}{r^2} + p_\gamma\left(\frac{v^2}{r}-\frac{1}{r^2}\right)\frac{\sin\gamma}{v} \quad (10)$$

$$\frac{dp_J}{d\tau} = 0. \quad (11)$$

Introducing the control variables C and S for convenience,

$$C = \Gamma\cos\delta_t \quad (12)$$

$$S = \Gamma\sin\delta_t, \quad (13)$$

the optimal control according to the Maximum Principle is given by

$$C^* = -\frac{p_v}{p_J} \quad (14)$$

$$S^* = -\frac{p_\gamma}{vp_J}. \quad (15)$$

These controls globally maximize the Hamiltonian. This is the trajectory variable form of the coordinate-free result for minimum-fuel, LP transfer: the optimal thrust vector is equal to the primer vector [6].

The optimal Hamiltonian is given by

$$H^* = p_r v\sin\gamma + p_\theta\frac{v\cos\gamma}{r} - p_v\frac{\sin\gamma}{r^2} + p_\gamma\left(\frac{v^2}{r}-\frac{1}{r^2}\right)\frac{\cos\gamma}{v} - \frac{1}{2p_J}\left(p_v^2+\frac{p_\gamma^2}{v^2}\right). \quad (16)$$

Since H^* does not depend explicitly on time, and θ and J are ignorable, there exist the following first integrals

$$H^* = c_1 \quad (17)$$

$$p_\theta = c_2 \quad (18)$$

$$p_J = c_3 = -1. \quad (19)$$

The adjoint $p_J = -1$ since J is being minimized. A fourth integral of the motion [6], which can be verified by differentiation, is

$$2rp_r - vp_v = 3H^*\tau - 5J + c_4. \quad (20)$$

The initial and final conditions for the coplanar transfer problem are specified in terms of the nondimensional orbital elements, semimajor axis α or energy ξ, which have been nondimensionalized using r_{ref}, eccentricity e, and argument of periapse ω. The transformations between trajectory variables and classical orbit elements are well-known [17].

The initial energy ξ_0, initial eccentricity e_0, and initial argument of periapse ω_0 are specified. The departure point on the initial orbit is chosen to be periapse. The sensitivity of the tranfer cost to the departure point decreases as the transfer time increases. We have not optimized the departure point in this paper. The general final conditions for a coplanar transfer are that the final energy $\xi(\tau_f)$, final eccentricity $e(\tau_f)$, and final argument of periapse $\omega(\tau_f)$ match the specified final values ζ_f, e_f, and ω_f. In terms of the trajectory variables, these conditions can be expressed as

$$\Psi_1 = \xi(\tau_f) - \xi_f = \frac{v(\tau_f)^2}{2} - \frac{1}{r(\tau_f)} - \xi_f = 0 \quad (21)$$

$$\Psi_2 = e(\tau_f) - e_f = \sqrt{1+2\xi(\tau_f)p(\tau_f)} - e_f = 0 \quad (22)$$

$$\Psi_3 = \omega(\tau_f) - \omega_f = \theta(\tau_f) - \arctan\left(\frac{p(\tau_f)\tan\gamma(\tau_f)}{p(\tau_f)-r(\tau_f)}\right) - \omega_f = 0, \quad (23)$$

where p is the semi-latus rectum. For transfers to or from a circle, the third constraint is ignored, since ω_f can be considered free.

The terminal conditions on the adjoint variables p_r, p_θ, p_v, and p_γ are given by

$$p_r(\tau_f) = -\mu_1\frac{\partial\Psi_1}{\partial r} - \mu_2\frac{\partial\Psi_2}{\partial r} - \mu_3\frac{\partial\Psi_3}{\partial r} \quad (24)$$

$$p_\theta(\tau_f) = \mu_3 \quad (25)$$

$$p_v(\tau_f) = -\mu_1\frac{\partial\Psi_1}{\partial v} - \mu_2\frac{\partial\Psi_2}{\partial v} - \mu_3\frac{\partial\Psi_3}{\partial v} \quad (26)$$

$$p_\gamma(\tau_f) = -\mu_2\frac{\partial\Psi_2}{\partial\gamma} - \mu_3\frac{\partial\Psi_3}{\partial\gamma}, \quad (27)$$

where μ_1, μ_2, and μ_3 are constant Lagrange multipliers. These equations can be combined, eliminating μ_1, μ_2, and μ_3 to form a transversality condition at the final time,

$$p_r(\tau_f) - \frac{1}{r(\tau_f)^2 v(\tau_f)}p_v(\tau_f) + \frac{1}{r(\tau_f)\tan\gamma(\tau_f)}p_\theta(\tau_f) + \frac{1}{r(\tau_f)\tan\gamma(\tau_f)}\left(1-\frac{1}{r(\tau_f)v^2(\tau_f)}\right)p_\gamma(\tau_f) = 0. \quad (28)$$

The three final state conditions along with this transversality condition, combined with the initial conditions on the state, are the boundary conditions for the transfer.

Equations (1)–(11), with the control replaced with the optimal expressions involving the adjoint variables [eqns (14)–(15)], define a Hamiltonian vector field on the state-adjoint space. The projection of an integral curve of the corresponding Hamiltonian flow onto the state space is an *extremal trajectory*. The Hamiltonian system is non-integrable in that there are five state variables and only four integrals of the motion [18]. For a sufficiently long transfer time, the system is only slightly perturbed from an integrable Hamiltonian system. The integrable system, whose behavior approximates the secular behavior of the system of interest, is obtained by the method of averaging [19]. The extremal trajectories of the integrable system provide much insight into the extremal trajectories for the system of interest. The trajectory variables must be replaced by slowly changing variables such as the classical orbit elements before the Hamiltonian system is in an appropriate form for the application of the averaging method. Rather than

re-deriving the necessary conditions in terms of the orbit elements, we can convert the necessary conditions as stated in trajectory variables to the necessary conditions as stated in orbit elements using a canonical transformation. The inverse transformation can then be used to convert results expressed in terms of the orbit elements into the corresponding results in trajectory variable form.

3. CANONICAL TRANSFORMATION TO ORBIT ELEMENTS

The transformation from trajectory variables to the classical orbit elements and the identity transformation of the fuel consumption variable J comprise the complete state variable transformation. Developing the transformation for the associated adjoint variables, p_a, p_e, p_ω, p_M, so that the differential one-form $\mathbf{p}\cdot\mathrm{d}\mathbf{x}$, where $\mathbf{x}$ represents the state and $\mathbf{p}$ represents the adjoint, is an invariant of the transformation is sufficient to ensure that the composite transformation of the ten state and adjoint coordinates is canonical, and, consequently, that extremal trajectories generated using the two sets of coordinates will be the same.

The derivations of the relevant canonical transformations are carried out in the Appendix.

4. APPROXIMATE INTEGRATION BY THE METHOD OF AVERAGING

By canonical transformation, the Hamiltonian can be expressed in the orbit elements and the associated adjoint variables

$$H^*(r, \theta, v, \gamma, J; p_r, p_\theta, p_v, p_\gamma, p_J) = F^*(\alpha, e, \omega, M, J; p_a, p_e, p_\omega, p_M, p_J). \quad (29)$$

F^* is a periodic function of M with period 2π. The remaining elements α, e, and ω, which define the size, shape, and orientation of the osculating orbit, respectively, and the fuel consumption variable J are slowly varying functions of time for long duration transfers; they are approximately constant over one cycle in M.

Exceptions to this are transfers involving near-circular orbits. There is a singularity in the rate of change of ω when $e = 0$. Although averaging results can be obtained formally for $e = 0$ by taking limits, the accuracy of the solution may degrade for transfers involving near-circular orbits. Nonetheless, we are employing the classical orbit elements initially in order to maintain continuity with the previous work [6,9,10].

The *average Hamiltonian* is defined as [6,10]

$$\bar{F}^*(\alpha, e, \omega, J; p_a, p_e, p_\omega, p_M, p_J) = \frac{1}{2\pi}\int_0^{2\pi} F^*(\alpha, e, \omega, M, J; p_a, p_e, p_\omega, p_M, p_J)\,\mathrm{d}M, \quad (30)$$

and the corresponding average vector field is

$$\frac{\mathrm{d}\bar{\mathbf{x}}}{\mathrm{d}\tau} = \frac{\mathrm{d}\bar{F}^*}{\mathrm{d}\mathbf{p}} \quad (31)$$

$$\frac{\mathrm{d}\bar{\mathbf{p}}}{\mathrm{d}\tau} = -\frac{\mathrm{d}\bar{F}^*}{\mathrm{d}\mathbf{x}}, \quad (32)$$

where $\bar{}$ denotes an average quantity. An integral curve of the average vector field is expressed using the average coordinates $\bar{\alpha}, \bar{e}, \bar{\omega}, \bar{J}, \bar{p}_a, \bar{p}_e, \bar{p}_\omega$, and $\bar{p}_M$. The *average* minimum-fuel transfer boundary value problem approximating the exact minimum-fuel transfer boundary value problem is obtained by replacing eqns (2)–(11) with eqns (31) and (32) and rewriting the boundary conditions in terms of the average coordinates. The average minimum-fuel transfer approximates the secular changes in the *exact* minimum-fuel transfer.

The four integrals given in eqns (17)–(20) can be written in terms of the orbit elements and their adjoint variables. By replacing these coordinates with the corresponding average coordinates, four integrals for the average system are obtained [11]. Since M does not appear in the average Hamiltonian, there is the fifth integral

$$\bar{p}_M = c_5. \quad (33)$$

For an orbit transfer, as opposed to a rendezvous, $M(\tau_f)$ is unspecified, and we have the transversality condition $p_M(\tau_f) = 0$, or, for the average system, $\bar{p}_M(\tau_f) = 0$. Hence, c_5 is zero and $\bar{p}_M$ is identically zero for the average system. With five integrals, the average Hamiltonian system is integrable; i.e. the differential eqns (31)–(32) can be integrated by quadratures.

The integration problem is greatly simplified by noting [6,9] that it can be divided into two decoupled and simpler subproblems. The first involves the size and fuel consumption variables, $\bar{\alpha}$ and $\bar{J}$; the second involves the shape and orientation variables, $\bar{e}$ and $\bar{\omega}$. The first problem lends itself to straightforward integration and, based on the solution, the following general conclusions regarding the *secular* behavior follow [6,9]:

(1) The optimal thrust magnitude is constant.
(2) The fuel consumption is a linear function of time.
(3) The semimajor axis (or equivalently the energy) is either monotonic (increasing or decreasing) or passes through a maximum.
(4) The thrust level is inversely proportional to the transfer time.

For the transfer between coplanar ellipses, the shape-orientation subproblem can be solved in terms of elementary functions; thus, solving the boundary value problem for the extremal trajectories reduces to solving a system of nonlinear algebraic equations. A complete derivation of the averaging solution for transfer between coplanar ellipses as well as details

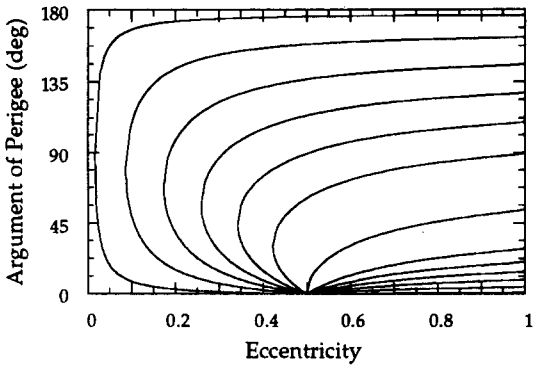

Fig. 1. Average extremals for initial conditions, $\bar{e}_0 = 0.5$ and $\bar{\omega}_0 = 0$.

concerning the calculations of the averaging results presented in Fig. 1 and the following sections can be found in [20].

Figure 1 shows the field of extremals for the shape-orientation coplanar transfer subproblem corresponding to the initial conditions $\bar{e}_0 = 0.5$ and $\bar{\omega}_0 = 0$ deg. By considering the ordinate as the change in $\bar{\omega}$, the figure encompasses all initial values of $\bar{\omega}$. The extremals leading to $\bar{\omega} \in (0, -180)$ are obtained by reflection with respect to $\bar{\omega} = 0$ [6]. Edelbaum [9] contains a similar plot except that transfers during which the direction of motion in the orbit reverses are considered. Direction reversals occur as the osculating orbit passes through the condition $\bar{e} = 1$, i.e. when the osculating orbit is a rectilinear ellipse. We do not consider transfers involving a passage through a rectilinear ellipse in this paper. There are two qualitatively distinct types of extremals—those that begin with $\bar{e}$ decreasing and those that begin with $\bar{e}$ increasing (Fig. 1). An explicit formula exists for computing the extremal that separates these two types of motion.

By disallowing direction reversals, there remains a unique extremal connecting the initial point to every other point in the $\bar{e}$–$\bar{\omega}$ plane, and no points conjugate to the initial point are encountered on the extremal [9]. Thus, the extremals are globally minimizing for the class of transfer under consideration. This statement holds not only for the initial eccentricity shown in Fig. 1 but also for any initial eccentricity between zero and one. The projection of the average extremal trajectories onto the $\bar{e}$–$\bar{\omega}$ plane is independent of the final time, so the statement holds for all final times. For a given final time, there is a unique extremal in the four dimensional $(\bar{\alpha}, \bar{e}, \bar{\omega}, J)$ space that corresponds to the projection on the $\bar{e}$–$\bar{\omega}$ plane. It follows that *the extremals computed for the average system are globally minimizing within the class of transfers having no direction reversals.*

The average extremals thus provide a comprehensive picture of the minimum-fuel trajectories for the average system: the qualitative features of the optimal trajectories are clear, and the trajectories are readily computed from algebraic equations. For long duration transfer, a close quantitative correspondence is expected between the minimum-fuel trajectories for the average system and those for the exact system. However, as the transfer time decreases and higher thrust levels are experienced, the quantitative, and perhaps even the qualitative, correspondence between the minimum-fuel trajectories of the average system and those of the exact system can break down. Averaging theory [21] says that the difference between the exact and average state variables will be $O(\epsilon)$ on an $O(1/\epsilon)$ time interval, where ϵ is the constant average nondimensional thrust acceleration. (An error $\Delta(\epsilon)$ is $O(\epsilon)$ for $\epsilon \to 0$ if there exists a constant k such that $|\Delta(\epsilon)| \leqslant k\epsilon$ for $\epsilon \to 0$ [21].) The exception is M, the variable over which the averaging is done. The mean anomaly $\bar{M}$ for the average system is an ignorable coordinate; it is given in the form of a quadrature involving the other average variables. In contrast to the other average variables, the error in $\bar{M}$ is $O(1)$[11,21].

In the following sections, we show that the qualitative correspondence between the minimum-fuel trajectories of the average system and those of the exact system does not break down as the transfer time decreases for transfers with at least two revolutions. Furthermore, we show how the average solutions can be used to generate the non-secular behavior—in particular, the behavior of the thrust magnitude and direction during individual revolutions—and to generate near minimum-fuel solutions for the exact system.

5. APPROXIMATE INITIAL ADJOINT AND FEEDBACK CONTROL IN TRAJECTORY VARIABLES

Using the canonical transformation between the orbit elements and trajectory variables (see Appendix for derivation), approximations for the adjoint variables associated with the trajectory variables can be obtained. Let $\hat{}$ denote an approximation of a variable associated with the exact system. Substituting the average adjoint variables into eqns (A49)–(A54), recalling that $\bar{p}_M \equiv 0$, gives

$$\hat{p}_r = \frac{2\alpha^2}{r^2}\bar{p}_\alpha + \left[\bar{p}_e + \frac{\bar{p}_\omega \sin f}{e(e+\cos f)}\right]\frac{(e+\cos f)}{r} \tag{34}$$

$$\hat{p}_\theta = \bar{p}_\omega \tag{35}$$

$$\hat{p}_v = 2\alpha^2 v\bar{p}_\alpha + \left[\bar{p}_e + \frac{\bar{p}_\omega \sin f}{e(e+\cos f)}\right]\frac{2(e+\cos f)}{v} \tag{36}$$

$$\hat{p}_\gamma = \frac{\bar{p}_e(1-e^2)\sin f}{(1+e\cos f)} - \frac{\bar{p}_\omega}{e(1+e\cos f)} \times [e(1+e\cos f) + (e+\cos f)], \tag{37}$$

where the true anomaly f has been introduced. These equations are expressed in terms of both orbital elements and trajectory variables for simplicity. For a specified transfer, the average adjoint variables can be computed and substituted into these equations

along with the exact initial conditions for the state variables to generate approximations to the exact initial adjoint variables. An extremal solution can be generated by numerically integrating the state and adjoint equations. This extremal solution will satisfy the terminal constraints as $\epsilon \to 0$.

Alternatively, $\hat{p}_v$ and $\hat{p}_\gamma$ can be substituted into eqns (14) and (15) to obtain the optimal control laws,

$$\hat{C} = 2\alpha^2 v\bar{p}_\alpha + \left[\bar{p}_e + \frac{\bar{p}_\omega \sin f}{e(e+\cos f)}\right]\frac{2(e+\cos f)}{v} \quad (38)$$

$$\hat{S} = \frac{\bar{p}_e(1-e^2)\sin f}{(1+e\cos f)v} - \frac{\bar{p}_\omega}{ev(1+e\cos f)} \times [e(1+e\cos f)+(e+\cos f)]. \quad (39)$$

For a given final orbit, $\bar{p}_\alpha$, $\bar{p}_e$, and $\bar{p}_\omega$ are easily computed functions of the current state, so eqns (38) and (39) can be considered an approximate feedback law for the optimal control.

Notice that the equations for $\hat{p}_r$, $\hat{p}_v$, and $\hat{p}_\gamma$ are not well-defined for $e = 0$. The condition $e = 0$ occurs when transferring to or from a circle. The appropriate equations for $e = 0$ are obtained by taking the limit as $e \to 0$

$$\lim_{e\to 0}\hat{p}_r = \frac{2\alpha^2}{r^2}\bar{p}_\alpha + \bar{p}_e\frac{\cos f}{r} + \lim_{e\to 0}\left(\frac{\bar{p}_\omega \sin f}{er}\right) \quad (40)$$

$$\lim_{e\to 0}\hat{p}_v = 2\alpha^2 v\bar{p}_\alpha + \frac{2\bar{p}_e\cos f}{v} + \lim_{e\to 0}\left(\frac{2\bar{p}_\omega \sin f}{ev}\right) \quad (41)$$

$$\lim_{e\to 0}\hat{p}_\gamma = \bar{p}_e \sin f - \bar{p}_\omega - \lim_{e\to 0}\frac{\bar{p}_\omega \cos f}{e}. \quad (42)$$

Consider the limit as $e \to 0$ of $\bar{p}_\omega/e$. Since $\bar{p}_\omega \equiv 0$ for a transfer to or from a circle [6,20] l'Hopital's rule is used to determine the limit:

$$\lim_{e\to 0}\frac{\bar{p}_\omega}{e} = \lim_{e\to 0}\frac{d\bar{p}_\omega/d\tau}{de/d\tau}. \quad (43)$$

Because $\bar{p}_\omega \equiv 0$, all derivatives of $\bar{p}_\omega$ with respect to τ are zero. Since $e \equiv 0$ is not possible for a coplanar transfer, we know that if $de/d\tau = 0$, some higher derivative of e with respect to τ will not be zero. Thus, by applying l'Hopital's rule an appropriate number of times, the limit is

$$\lim_{e\to 0}\frac{\bar{p}_\omega}{e} = 0, \quad (44)$$

and the approximate adjoint variables reduce to

$$\hat{p}_r = \frac{2\alpha^2}{r^2}\bar{p}_\alpha + \bar{p}_e\frac{\cos f}{r} \quad (45)$$

$$\hat{p}_v = 2\alpha^2 v\bar{p}_\alpha + \frac{2\bar{p}_e\cos f}{v} \quad (46)$$

$$\hat{p}_\gamma = \bar{p}_e \sin f. \quad (47)$$

When both the initial and final orbits are circles, $\bar{p}_e \equiv 0$[6,20], and the equations further reduce to

$$\hat{p}_r = \frac{2\alpha^2}{r^2}\bar{p}_\alpha \quad (48)$$

$$\hat{p}_v = 2\alpha^2 v\bar{p}_\alpha \quad (49)$$

$$\hat{p}_\gamma = 0. \quad (50)$$

The approximate feedback law for departure from a circle is calculated by substituting eqns (46) and (47) into eqns (14) and (15). For the special case of transfer between two circles, substitute eqns (49) and (50) into eqns (14) and (15) to obtain the tangential thrust program

$$\hat{T} = 2r^2 v\bar{p}_\alpha \quad (51)$$

$$\hat{\delta}_t = 0. \quad (52)$$

6. ACCURACY OF THE APPROXIMATIONS

Two approximate methods for obtaining minimum-fuel trajectories for the exact system based on the solutions for the average system are proposed. In the first, the approximate initial adjoint is used to generate an extremal trajectory by integrating the state and adjoint equations. In the second, the approximate feedback law for the optimal control is used to generate an approximate minimum-fuel trajectory by providing the control as the state equations are integrated.

The accuracy of the approximate initial adjoint is investigated by generating a variety of transfers and looking at how well the final conditions are satisfied. Since the trajectories generated using the approximate initial adjoint are already extremal trajectories, this is all that is needed. The accuracy of the approximate feedback law is investigated by generating a similar set of transfers. The initial and final transfer orbits and transfer times are chosen to correspond to transfer orbits and transfer times of the extremal trajectories generated when investigating the accuracy of the approximate initial adjoint. The approximate feedback trajectories can then be compared to these extremal trajectories. Not only is the satisfaction of the final conditions considered, but also how well the feedback control approximates the extremal control and how closely the costs of the transfers match.

6.1. Approximate initial adjoint

The accuracy of the approximate initial adjoint is determined for a range of transfers, including circle to circle, circles to ellipse, and ellipse to ellipse transfers. For the transfers between circles the final radius was 1.5 times the initial radius, and the transfer times ranged from 1900 to 1.9. These transfer times corresponded to average thrust acceleration levels ϵ from 10^{-4} to 10^{-1}. For the transfers between circles and ellipses, two types of transfer were

considered. In the first the transfer time was fixed at 190($\epsilon \sim 10^{-3}$) and the final eccentricity ranged from 0.1 to 0.7. In the second, the final eccentricity was fixed at 0.3, and the transfer times ranged from 1900 to 1.9 ($\epsilon \sim 10^{-4}$–10^{-1}). For the transfers between ellipses, two types of transfer were considered; in both the line of apsides was rotated 30 deg. In the first the transfer time was fixed at 200 ($\epsilon \sim 10^{-3}$) and the initial (and final) eccentricity ranged from 0.1 to 0.9. In the second the initial (and final) eccentricity was fixed at 0.1 and the transfer time ranged from 2000 to 2 ($\epsilon \sim 10^{-4}$–10^{-1}).

The approximate initial adjoint is very accurate overall. For transfers ranging from a few to hundreds of revolutions, the final conditions are usually satisfied to within 10% of the desired values. In many cases, the approximate initial adjoint is so accurate that further refinement using a numerical optimization method is unnecessary. The approximate initial adjoint is particularly accurate for transfers between ellipses where the initial and final eccentricities are >0.1.

In general, as the transfer time decreases, the accuracy with which the final conditions are met decreases. For transfers between circles and ellipses with a fixed transfer time where $e_f > 0.1$, the accuracy of the final conditions decreases as the final eccentricity of the transfer increases. This is also the case for the rotation of the line of apsides of an ellipse when the transfer time is fixed. As the initial (and final) eccentricity increases, the accuracy of the final conditions decreases. For the same transfer time and roughly the same final eccentricity, the final conditions for the rotation of an ellipse are satisfied better than the final conditions for the transfer between a circle and an ellipse.

6.2. *Approximate feedback*

The accuracy of the approximate feedback law is assessed for a similar set of transfers, including transfers from circles to near circles, circles to ellipses, and ellipses to ellipses. For the transfers between circles and near circles, the final eccentricity was less than 0.05, the final semimajor axis was 1.5 times the initial semimajor axis, and the transfer times ranged from 1900 to 19, corresponding to thrust acceleration levels from 10^{-4} to 10^{-2}. For the transfers between circles and ellipses two types of transfers were considered. In the first the transfer time was fixed at 190 ($\epsilon \sim 10^{-3}$) and the final eccentricity ranged from 0.1 to 0.6. In the second, the final eccentricity was fixed at 0.3 to 0.4, and the transfer times ranged from 1900 to 19 ($\epsilon \sim 10^{-4}$–10^{-2}). For the transfers between ellipses, two types were tested; in both types the line of apsides was rotated 30 deg. In the first the transfer time was fixed at 200 ($\epsilon \sim 10^{-3}$) and the initial (and final) eccentricity ranged from 0.1 to 0.9. In the second the initial (and final) eccentricity was fixed at 0.1 and the transfer time ranged from 2000 to 20 ($\epsilon \sim 10^{-4}$–10^{-1}).

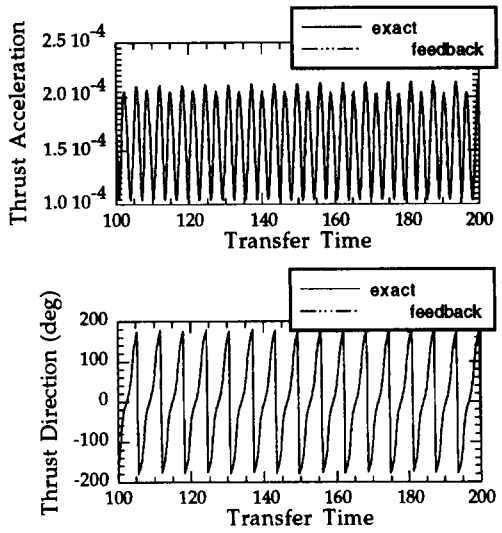

Fig. 2. Comparison of approximate feedback and exact thrust profiles for the rotation of the line of apsides of an ellipse ($\alpha_f = \alpha_0$; $e_0 = e_f = 0.1$). Second half of the transfer is shown.

The final conditions are satisfied extremely well when using approximate feedback; the accuracy follows the same pattern as the approximate initial adjoint. The accuracy decreases as the transfer time decreases and/or the final eccentricity of the transfer increases, where $e_f > 0.1$. For the same transfer time and final eccentricity, the final conditions are not satisfied as well when departing from a circle as when departing from a moderate eccentricity ellipse.

The approximate feedback control matches the exact control for certain types of transfers. For transfers between ellipses of moderate eccentricity, the correspondence is excellent, as illustrated in Fig. 2 for the 30 deg rotation of an ellipse with $e_0 = e_f = 0.1$. The second half of the transfer is shown; the correspondence is as good for the first half. This

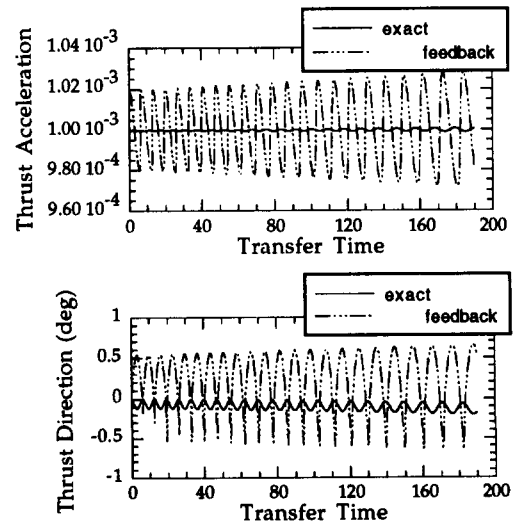

Fig. 3. Comparison of approximate feedback and exact thrust profiles for the transfer between a circle and a nearly circular orbit ($\alpha_f = 1.5\alpha_0$; $e_f = 0.006$).

excellent correspondence degrades as the eccentricity of the terminal ellipse increases, however. Although the control matches well at the beginning of the transfer, a phasing problem develops as the transfer progresses, so that by the end of the transfer, the approximate transfer has a different number of revolutions than the exact transfer. For the $e_0 = e_f = 0.9$ and $\tau_f = 200$, an extreme example because of the high eccentricities, the feedback transfer has 37 revolutions while the extremal transfer has 34. Despite this difference in the number of revolutions, however, the cost of the approximate transfer is within 1% of the cost for the exact transfer.

The feedback control does not approximate the exact control as well for transfers between circles and ellipses, as shown in Fig. 3. Although the feedback control and extremal control both oscillate, the oscillations are much larger in the feedback case. In addition, these oscillations are not in phase with the extremal solution. Despite this difference in control, however, the cost is within 2% of the cost for the exact transfers between circles and ellipses with thrust acceleration levels ranging from 10^{-4} to 10^{-2}.

6.3. *Assessment of the approximations*

The approximations are most accurate for low thrust acceleration and degrade as thrust acceleration increases (transfer time decreases). Although only the error in the average adjoint affects the approximations directly, the error in the average state is also an indicator of how accurate the approximations should be. Since the error in $\bar{M}$ is $O(1)$, while the error in the other average state and adjoint variables is $O(\epsilon)$, the accuracy of the approximations is not strictly $O(\epsilon)$ but depends on the relative importance of $\bar{M}$ for a specific transfer. For the lowest thrust acceleration, 10^{-4} or less, the trajectories are sufficiently accurate that no further numerical refinement is necessary. For moderate thrust acceleration, 10^{-3}–10^{-2}, the trajectories may be sufficiently accurate, depending on the context, or could be used to initialize a numerical optimization algorithm for further refinement. Since the numerical solution of LP transfers becomes more difficult as transfer time increases (ϵ decreases), it is particularly advantageous that the approximations are so accurate for long transfer times.

The reduced accuracy for transfers involving circular or near circular orbits can be explained by examining the equation for $d\omega/d\tau$ used in the development of the averaging method [20]:

$$\frac{d\omega}{d\tau} = \epsilon \frac{\sqrt{\alpha(1-e^2)}}{e} \times \left(-\cos f \sin \delta_t + \frac{\sin f(2 + e \cos f)}{1 + e \cos f} \cos \delta_t \right). \quad (53)$$

This equation has an e in the denominator, which means that for low eccentricities, ω is changing very rapidly. But averaging is based on the assumption that α, e, and ω change slowly during a revolution. Since this is clearly violated when transferring to or from a circle or very low eccentricity ellipse, the adjoint obtained from averaging which is used in the approximations is not accurate. This problem could be overcome by developing an averaging solution using equinoctial elements.

The decrease in accuracy for high eccentricity transfers is yet to be explained. As e increases, the number of revolutions in the feedback transfers does not match the number of revolutions in the extremal transfers. This problem may be related to the $O(1)$ error in $\bar{M}$.

The feedback law has potential application as a guidance law. The approximate initial adjoint variables $\bar{p}_\alpha$, $\bar{p}_e$, and $\bar{p}_\omega$ are computed *a priori* for a given transfer and only position and velocity are needed to computed the control. To account for perturbations such as drag or solar pressure, $\bar{p}_\alpha$, $\bar{p}_e$, and $\bar{p}_\omega$ could be recomputed periodically during the transfer using the current state information. Although the approximate feedback does not duplicate the exact control when the initial or final orbit is circular or highly elliptic, practically speaking this is not very important, since the final conditions are satisfied well and the fuel consumption is near minimum.

7. CHARACTERIZATION OF COPLANAR, MINIMUM-FUEL, POWER-LIMITED TRANSFERS

We have seen that minimum-fuel transfers for the average system are completely understood. The characterization of minimum-fuel transfers for the exact system would thus be in hand if it turned out that the exact transfers were well-approximated by the average transfers. Based on the study of a broad range of coplanar transfers between elliptic orbits with multiple revolutions, our overall conclusion is that the secular features of exact minimum-fuel, LP transfer are captured, at least qualitatively, by the average solution. As the transfer time increases, the quantitative correspondence improves. With the secular changes known and the fact that only small changes in the osculating elements occur during any given revolution, the analytic theory for infinitesimal transfer [8] can be used to determine the behavior of the elements and the thrust during the course of a revolution. It is interesting that an approximate solution more accurate than the average solution discussed in this paper, called the *improved first approximation* [22] is indeed constructed by combining the solution for infinitesimal transfer with the average solution [23]. We do not have any experience with the improved first approximation, but it appears worthy of further study.

The approximate initial adjoint method is used to generate the transfers that are compared to the average transfers. The method produces extremal trajectories, to within the precision of the numerical

integration. The transfers are approximate in that the specified final orbits are not achieved. However, for our purposes, we can simply adjust the final conditions, after the fact, so that the extremal transfers produced do satisfy the final conditions. We refer to transfers computed in this manner as *exact*. Once an extremal transfer has been determined in this manner, the average transfer corresponding to the adjusted final orbit is computed and compared to the exact transfer.

The transfers discussed in detail in the remainder of this section are selected to illustrate certain generic features of the many transfers studied. The first part of the discussion focuses on comparing the size, shape, and orientation of some selected transfers with the predictions from averaging. Although the orbit elements are used in the discussion, the numerical integration uses trajectory variables. The second part of the discussion focuses on the characteristic thrust profiles for three specific transfers: transfer from a circle to a nearly circular orbit, a circle to an ellipse, and the rotation of the line of apsides of an ellipse. Polar plots of these transfers are shown in Fig. 4.

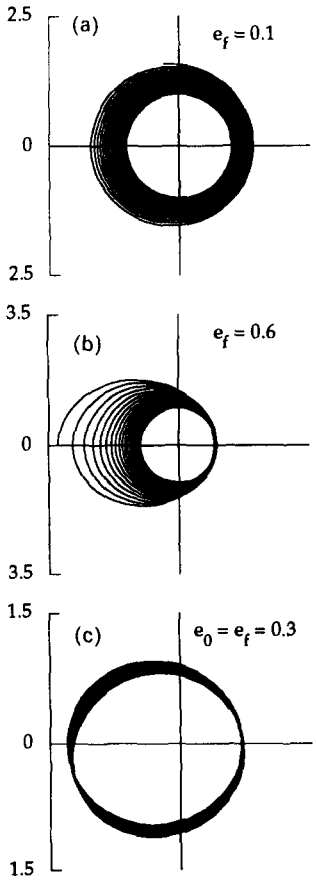

Fig. 4. Polar view of three transfers. (a) Circle to ellipse, $e_f = 0.1$; (b) circle to ellipse, $e_f = 0.6$; (c) rotation of an ellipse, $e_0 = e_f = 0.3$.

Table 1. Example transfers

Description	Transfer time	Avg. thrust accel	No. of revs
Circle/ellipse, $e_f = 0.1$	190	10^{-3}	22
Circle/ellipse, $e_f = 0.6$	190	10^{-3}	19
Rotation of ellipse, $e_0/e_f = 0.3$	200	10^{-4}	32

7.1. Size, shape, and orientation characteristics

Consider the 30 deg rotation of an ellipse with $e_0 = e_f = 0.3$. A polar view of this transfer is given in Fig. 4(c), and the transfer time, average thrust acceleration, and the number of revolutions are given in Table 1. Time histories of α, e, and ω are shown in Fig. 5. The exact orbit elements are compared with $\bar{\alpha}$, $\bar{e}$ and $\bar{\omega}$. The average semimajor axis increases slightly and then decreases monotonically to the final value. The exact semimajor axis oscillates. Each oscillation corresponds to one revolution of the transfer. The mean behavior is an increase in α followed by a decrease to the final value. The increase in α is larger than that predicted by averaging but only by 0.5%. The average eccentricity decreases monotonically to a minimum at the midpoint of the transfer and then increases monotonically. The exact eccentricity oscillates about the average value. The oscillations are small, and e oscillates twice per revolution. The average and exact arguments of periapse are almost indistinguishable. The exact argument of periapse oscillates very slightly about $\bar{\omega}$.

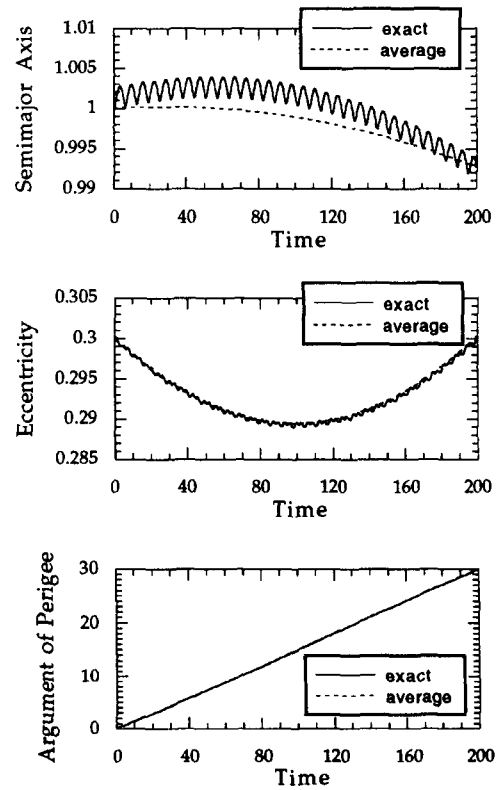

Fig. 5. A comparison of the average and exact orbital elements for the 30 deg rotation of an ellipse, $e_0 = e_f = 0.3$.

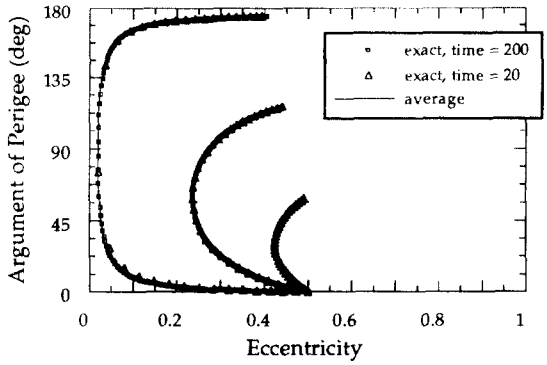

Fig. 6. Comparison of average and exact extremals for two transfer times, $e_0 = 0.5$.

As the transfer time decreases by an order of magnitude, the number of revolutions also decreases by an order of magnitude, while the average thrust acceleration increases by an order of magnitude. In addition, the sizes of the oscillations in the extremal solution increase as the transfer time decreases. These properties are true of all multiple revolution LP transfers.

There is an alternate way of viewing the evolution of e and ω during a transfer. Instead of looking at time histories, the argument of perigee can be plotted vs the eccentricity to generate an extremal for the shape-orientation subproblem. For the exact transfers, e and ω are not plotted for all time points. Instead, e and ω are sampled at $f = 0 \pmod{2\pi}$ and these discrete points are plotted. This removes the oscillation during each revolution and shows only the secular behavior. A plot of the extremals is shown in Fig. 6 for three transfers starting from an ellipse with eccentricity 0.5. The line of apsides of this ellipse was rotated 60, 120, and 175 deg. The plot shows two different transfer times, 20 and 200, which correspond to average thrust acceleration of 10^{-3} and 10^{-4}, along with the average solution. As can be seen from the plots, which are representative for all the cases we have studies, *averaging predicts the secular orientation/shape accurately even for reasonably short duration transfers.*

7.2. Thrust profile characteristics

Thrust profiles are discussed for the three transfers shown in Fig. 4. These transfers were chosen to illustrate some characteristic features of the trajectories and thrust profiles of minimum-fuel, coplanar, LP transfers. The first transfer is between a circle and a low eccentricity ellipse with $e_f = 0.1$. The second transfer is between a circle and a moderate eccentricity ellipse with $e_f = 0.6$. The final transfer is the 30 deg rotation of the line of apsides of an ellipse, where $e_0 = e_f = 0.3$. The transfer times, average thrust accelerations, and number of revolutions for the three transfers considered are given in Table 1.

Transfer between a circle and low eccentricity ellipse. Time histories of the thrust profiles for the transfer between a circle and a low eccentricity ellipse are shown in Fig. 7. The thrust acceleration oscillates about a mean value. The thrust direction oscillates about zero degrees, i.e. about the direction of the velocity vector. Each oscillation in the thrust profile corresponds to one revolution in the transfer. This thrust profile is characteristic for transfers between circles and other circles or ellipses with eccentricity <0.2. It is also characteristic of transfers with different transfer times. As the transfer time decreases, the size of the oscillations of Γ and δ_t increases. For each order of magnitude decrease in the transfer time, there is a corresponding order of magnitude increase in the average thrust acceleration and order of magnitude decrease in the number of revolutions in the orbit.

Transfer between a circle and a moderate eccentricity ellipse. Time histories for the thrust profiles for the transfer between a circle and a moderate eccentricity ellipse with $e_f = 0.6$ are given in Fig. 8. At the

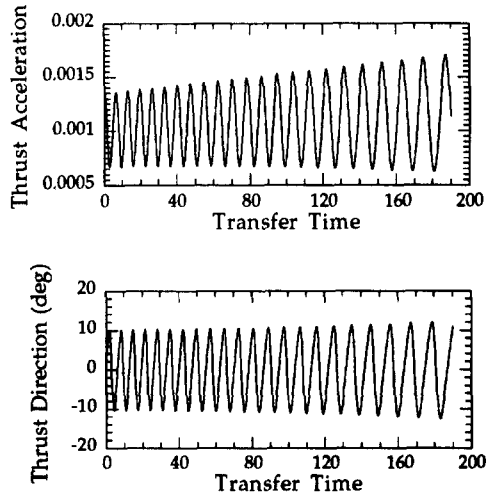

Fig. 7. Minimum-fuel thrust profiles for transfer between circle and ellipse, $e_f = 0.1$.

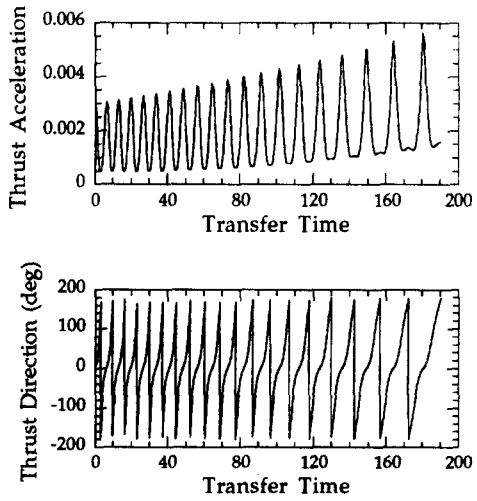

Fig. 8. Minimum-fuel thrust profiles for transfer between circle and ellipse, $e_f = 0.6$.

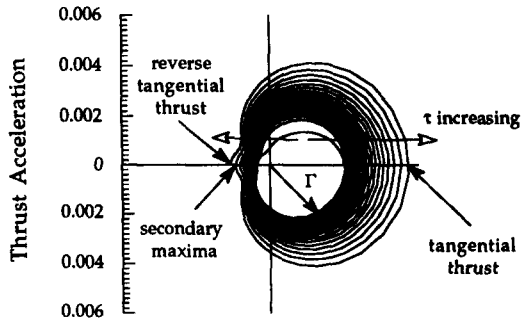

Fig. 9. Polar plot of thrust acceleration vs true anomaly for transfer between circle and ellipse, $e_f = 0.6$.

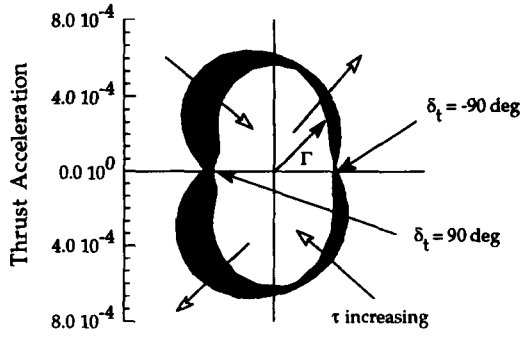

Fig. 11. Polar plot of thrust acceleration vs true anomaly for the 30 deg rotation of an ellipse, $e_0 = e_f = 0.3$.

beginning of the transfer, the thrust acceleration is very similar to the thrust acceleration for the transfer between a circle and low eccentricity ellipse. As the transfer progresses, however, secondary maxima appear. These secondary maxima become more pronounced as the transfer progresses. The thrust direction oscillates about zero, as in the circle/near circle case, but the oscillations are much larger, ranging between $+180$ and -180 deg. A ± 180 deg angle between the thrust vector and the velocity vector corresponds to reverse thrust.

To determine the behavior of the thrust during each revolution, the thrust acceleration is plotted on a polar plot using f as the angle, where $0 \leqslant f \leqslant 360$ deg. Recall that $f = 0$ corresponds to the periapse and $f = 180$ deg corresponds to the apoapse of the osculating orbit. Figure 9 shows the thrust acceleration vs f. The trends as τ increases are shown with arrows. The maximum Γ occurs at periapse and the minimum at apoapse, and Γ is symmetric about the major axis. The secondary maxima are apparent on this plot; they occur at apoapse. The important features of the thrust direction are also labelled.

The thrust direction is zero at periapse and 180 deg at apoapse. In other words, the thrust is in the direction of the velocity vector at periapse and reversed at apoapse. The thrust direction is antisymmetric about the major axis; i.e. $\delta_t(f) = -\delta_t(360 \text{ deg} - f)$. A view of the thrust vector for one osculating orbit is shown pictorially by drawing one osculating orbit with the thrust vectors at apoapse, periapse and some intermediate points (Fig. 10). The size of the thrust vectors is exaggerated for emphasis.

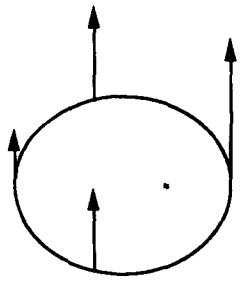

Fig. 10. Polar view of thrust vectors over one osculating orbit for transfer between circle and ellipse, $e_f = 0.6$.

The behavior of the thrust during a revolution can be compared to Edelbaum's results for infinitesimal transfers [8] since the orbit changes are small. From Edelbaum's results, when α is increased while holding the other orbit elements fixed, the thrust is always in the direction of the velocity. The thrust magnitude is a maximum at periapse and a minimum at apoapse. When e is increased while holding the other orbit elements fixed, the thrust magnitude is a maximum at periapse and apoapse and a minimum in between. The thrust is tangential at both periapse and apoapse, although the direction is reversed at apoapse. The thrust direction is positive when $f < 180$ deg.

The thrust profiles shown in Figs 8–10 are typical for transfers between circles and ellipses with $e > 0.3$. As e_f increases, the size of the reverse thrust at apoapse increases and begins earlier in the transfer. As the transfer time decreases, the magnitude of the thrust acceleration increases and the number of revolutions decreases, but the shape of the polar plots of the thrust profiles vs f stays the same.

For the circle to ellipse transfers considered here, both α and e increase. Therefore the transfers between a circle and an ellipse are expected to be a combination of Edelbaum's results for an increase in α and an increase in e. The thrust magnitude should be a maximum at periapse and a minimum at apoapse. The thrust direction should be 0 deg at periapse, 180 deg at apoapse, and positive when $f < 180$ deg. These qualitative predictions are consistent with Figs 9 and 10.

Rotation of the line of apsides of an ellipse. Polar plots of the thrust acceleration vs f are shown in Fig. 11 for the 30 deg rotation of the line of apsides of an ellipse. The trends as τ increases are shown with

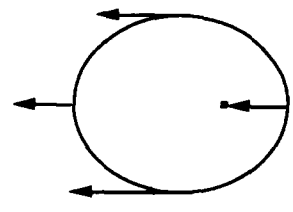

Fig. 12. Polar view of thrust vectors over one osculating orbit for 30 deg rotation of an ellipse, $e_0 = e_f = 0.3$.

arrows, and the important features of the thrust direction are labelled. A polar view of the thrust vectors for one osculating orbit is shown in Fig. 12. The size of the thrust vectors is exaggerated for emphasis. The thrust accleration has two maxima and two minima during each revolution of the transfer, rather than one of each as in the case of the transfer between a circle and an ellipse. The thrust acceleration is symmetric about the major axis and passes through the maximum between the latus rectum and apoapse. At the start of the transfer, the maximum between $f = 90$ deg and $f = 180$ deg is the largest. This maximum decreases as τ increases. The maximum between $f = 180$ deg and $f = 270$ deg starts out smaller but increases as the transfer progresses until midway through the transfer it is the largest. δ_t is positive around apoapse and negative around periapse. The point of transition from δ_t positive to δ_t negative changes as the transfer evolves.

These results are consistent with Edelbaum's linearized transfers if the transfer is considered to be primarily a change in ω with the increase and decrease in e overlaid. The change in α is so small it can be ignored in this qualitative analysis. When e is increased while holding the other orbit elements fixed, the thrust magnitude is a maximum at periapse and apoapse and a minimum in between. The thrust is tangential at both periapse and apoapse, although the direction is reversed at apoapse. The thrust direction is positive when $f < 180$ deg. When ω increases while holding the other orbit elements fixed, the thrust magnitude is a minimum at periapse and apoapse and symmetric about the major axis. The thrust direction $\delta_t = -90$ deg at periapse and 90 deg at apoapse.

The rotation of the line of apsides of an ellipse is a combination of Edelbaum's results for an increase in ω and an increase in e. The change in ω is the dominant feature, so the thrust profiles should correspond to an increase in ω with a correction for the decrease in e for the first half of the transfer and a correction for the increase e for the second half of the transfer. The thrust acceleration is a minimum at periapse and apoapse, as expected (Fig. 11). The thrust direction varies from -100 deg to -80 deg at periapse. Edelbaum's results predict -90 deg. δ_t starts at -100 deg instead of -90 deg because e is also decreasing, and a decrease in e is achieved with a tangential reverse thrust at periapse. As the transfer progresses, the decrease in e during a revolution lessens so δ_t increases to -90 deg until e reaches its minimum value midway through the transfer. At this point e begins to increase, which is achieved by a thrust along the velocity vector at periapse, causing δ_t to increase until it reaches -80 deg at the end of the transfer. Similar reasoning explains the behavior at apoapse, where δ_t starts at 80 deg and increases to 100 deg.

The change in e at the same time that ω is increasing also causes the asymmetry in Γ over each orbit. Γ is symmetric about the major axis for both an increase in e and an increase in ω. However $\delta_t(f) = -\delta_t(360 \text{ deg} - f)$ when e changes, while $\delta_t(f) = -(180 \text{ deg} + \delta_t(360 \text{ deg} - f)$ when ω changes. Therefore, when the thrust vectors are added, the symmetry in Γ is not preserved. When e is decreasing, the second maximum in each orbit is smaller; when e is increasing, the first maximum is smaller. The effect is more pronounced as e_0 $(= e_f)$ increases because the change in e during the transfer is greater.

8. CONCLUSIONS

A methodology has been developed for generating near minimum-fuel transfers between coplanar elliptic orbits for the LP propulsion model. The methodology is based on the method of averaging and canonical transformations. The exact Hamiltonian dynamical system, which with appropriate boundary conditions defines extremal transfers, is non-integrable. By averaging over a revolution, an integrable Hamiltonian system is obtained. The globally maximizing extremals for the integrable Hamiltonian system are easily computed and characterized. The non-secular behavior, which is suppressed by averaging, is recovered by using the solutions for the average adjoint variables and a canonical transformation to generate approximate initial adjoint variables. The exact Hamiltonian system is then integrated numerically with the approximate initial values to produce the approximate minimum-fuel transfer. If necessary, the computed transfer can be used to initialize a numerical optimization algorithm for further refinement.

The approximate and average minimum-fuel transfers are almost identical to the exact minimum-fuel transfers for long duration transfers with hundreds of revolutions that do not violate the assumptions underlying averaging. As the transfer duration decreases the quantitative correspondence degrades, although not dramatically. The approximate and average transfers are sufficiently accurate to characterize the qualitative properties of the exact minimum-fuel transfers for a wide range of transfer durations extending to short duration transfer with only a couple of revolutions. The average solution predicts qualitatively the correct secular behavior of the osculating orbit, while the approximate solution supplies the non-secular behavior—in particular, the behavior of the optimal thrust magnitude and direction during each revolution. The qualitative behavior of the control during a revolution is consistent with the analytical results for infinitesimal transfers. An important consequence of the qualitative accuracy of the average solution is that the clear understanding of the normally difficult issues of nonuniqueness, local vs global optimality, and conjugate points gained from the average solution applies

to minimum-fuel transfers of both long and short duration.

Some recommendations for further study are these. First, the average solutions predict the secular evolution of the shape and orientation of the osculating orbit accurately for a wide range of transfer durations. On the other hand, the accuracy with which the secular behavior of the orbit size is predicted decreases as the transfer duration decreases. Thus, it may be possible to improve the overall accuracy of the solution by improving the solution of the size-cost subproblem. Also, the accuracy of the improved first approximation, which combines the average solution with the solution for infinitesimal transfer, should be evaluated. Second, the singularities associated with the classical elements are a source of error in the average solutions that could be eliminated by employing nonsingular elements such as the equinoctial elements. Third, the lower accuracy of the average solutions for transfers involving large eccentricity orbits needs to be explained. Fourth, the near-optimal feedback control law that has been developed using the solutions for the average adjoint variables should be evaluated as a candidate guidance law. Finally, the approach should be extended to three-dimensional transfers.

Acknowledgements—This research is sponsored by the NASA Lewis Research Center under grant NAG3-915 and the Department of Defense through a National Defense Science and Engineering Graduate Fellowship.

REFERENCES

1. R. G. Jahn, Electric propulsion. *Encyclopedia of Science and Technology*. Academic Press, New York. In press.
2. C. Sauer, Application of solar electric propulsion to future planetary missions. *DGLR/AIAA/JSASS 19th International Electric Propulsion Conference*, Colorado Springs, Colo. (1987).
3. K. T. Nock, TAU—a mission to a thousand astronomical units. *DGLR/AIAA/JSASS 19th International Electric Propulsion Conference*, Colorado Springs, Colo. (1987).
4. J. M. Sponable and J. P. Penn, Electric propulsion for orbit transfer—a NAVSTAR case study (has electric propulsion's time come?). AIAA 87-0985. *DGLR/AIAA/JSASS 19th International Electric Propulsion Conference*, Colorado Springs, Colo. (1987).
5. W. D. Deiniger and R. J. Vondra, Electric propulsion for constellation deployment and spacecraft maneuvering. AIAA 88-2833. *AIAA/ASME/SAE/ASEE 24th Joint Propulsion Conference*, Boston, Mass. (1988).
6. J.-P. Marec, *Optimal Space Trajectories*. Elsevier, Amsterdam (1979).
7. F. W. Gobetz, Optimal variable-thrust transfer of a power-limited rocket between neighboring circular orbits. *AIAA J.* **2**, 339–343 (1964).
8. T. N. Edelbaum, Optimal low-thrust rendezvous and station keeping. *AIAA J.* **2**, 1196–1201 (1964).
9. T. N. Edelbaum, Optimum power-limited orbit transfer in strong gravity fields. *AIAA J.* **3**, 921–925 (1965).
10. J.-P. Marec and N. X. Vinh, Optimal low-thrust, limited power transfers between arbitrary elliptical orbits. *Acta Astronautica* **4**, 511–540 (1977).
11. J.-P. Marec and N. X. Vinh, General study of optimal low thrust limited power transfers between arbitrary elliptical orbits. European Space Agency Report ESA-TT-697 (1981).
12. S. Ross and G. Leitmann, Low acceleration trajectory optimization in a strong central force field. *IAS Symposium on Vehicle Systems Optimization*, pp. 127–137. Institute of Aerospace Sciences, New York (1961).
13. K. D. Mease, C. M. Haissig and N. X. Vinh, Comparison of solution approaches for minimum-fuel, low-thrust, power-limited orbit transfers. AIAA 90-2960. *AIAA/AAS Astrodynamics Conference*. Portland, Ore. (1990).
14. A. Miele, *Flight Mechanics, Theory of Flight Paths*. Addison-Wesley, Reading, Mass. (1962).
15. N. X. Vinh, *Optimal Trajectories in Atmospheric Flight*. Elsevier, Amsterdam (1981).
16. K. D. Mease, S. H. Kuo and N. X. Vinh, Optimal plane change during constant altitude hypersonic flight. *J. Guidance* **14**, 797–806 (1991).
17. J. M. A. Danby, *Fundamentals of Celestial Mechanics*. Wilmann-Bell, Richmond, Va. (1988).
18. V. I. Arnold, *Mathematical Methods of Classical Mechanics*. Springer, New York (1989).
19. N. Kryloff and N. Bogoliuboff, *Averaging Methods in Nonlinear Dynamical Systems*. Princeton University Press, Princeton (1947).
20. K. D. Mease, N. X. Vinh, C. M. Haissig and N. Markopoulos, Optimal combination of orbit-changing mechanisms for space transportation. NASA Report (1989).
21. J. A. Sanders and F. Verhulst, *Averaging Methods in Nonlinear Dynamical Systems*. Springer, New York (1985).
22. N. N. Bogoliubov and Y. A. Mitropolsky, *Asymptotic Methods in the Theory of Non-linear Oscillations*. Hindustan, New Delhi (1961).
23. T. N. Edelbaum, An asymptotic solution for optimum power limited orbit transfer. *AIAA J.* **4**, 1491–1494 (1966).
24. W. F. Powers and B. D. Tapley, Canonical transformation applications to optimal trajectory analysis. *AIAA J.* **7**, 394–399 (1969).
25. D. F. Lawden, *Optimal Trajectories for Space Navigation*. Butterworths, London (1963).
26. G. A. Hazelrigg and P. M. Lion, Analytical determination of the adjoint vector for optimum space trajectories. *J. Spacecraft Rockets* **7**, 1200–1207 (1970).
27. D. C. Redding and J. V. Breakwell, Optimal low-thrust transfers to synchronous orbit. *J. Guidance Control Dynam.* **7**, 148–155 (1984).
28. C. G. Sauer Jr and W. G. Moyer, Optimum Earth-to-Mars roundtrip trajectories utilizing a low-thrust power limited propulsion system. *Adv. astronaut. Sci.* **13**, 547–570 (1963).
29. M. C. Bartholomew-Biggs, L. C. W. Dixon, S. E. Hersom and Z. A. Maany, The solution of some difficult problems in low-thrust interplanetary trajectory optimization. *Optimal Control applic. Meth.* **9**, 229–251 (1988).
30. P. J. Enright and B. A. Conway, Discrete approximations to optimal trajectories using direct transcription and nonlinear programming. AIAA 90-2963, *AIAA/AAS Astrodynamics Conference*, Portland, Ore. (1990).

APPENDIX

Canonical Transformation Between Orbit Elements and Trajectory Variables

The relationships between the orbit elements α, e, ω and M and the trajectory variables r, θ, v, and γ are well known [17]. To get the relationship between the corresponding adjoint

variables p_α, p_e, p_ω, and p_M and p_r, p_θ, p_v, and p_γ, a transformation preserving the invariance of the Hamiltonian must be developed. To develop this transformation, an intermediate set of elements in which the true anomaly f is used is introduced for convenience. The corresponding adjoint variables are p'_α, p'_e, p'_ω, and p'_f, where the primes have been added to avoid confusion with the adjoint variables p_α, p_e, p_ω, and p_M.

The canonical transformation between the orbit element adjoint and the trajectory variable adjoint is derived in two parts. First, the canonical transformation between p_r, p_θ, p_v, and p_γ and p'_α, p'_e, p'_ω, and p'_f is developed; then the canonical transformation between $p'_\alpha, p'_e, p'_\omega$, and p'_f and p_α, p_e, p_ω, and p_M is done. Both developments use the same general principle: the invariance of the Hamiltonian. For a change of state and adjoint $(\mathbf{x}_1; \mathbf{p}_1)$ to a new canonical set $(\mathbf{x}_2; \mathbf{p}_2)$ preserving the Hamiltonian, invariance of the Hamiltonian requires that [24]

$$\mathbf{p}_1 \cdot d\mathbf{x}_1 - \mathbf{p}_2 \cdot d\mathbf{x}_2 = 0. \tag{A1}$$

Canonical Transformation Between Trajectory Adjoint p_r, p_θ, p_v, p_γ and Orbit Adjoint p'_α, p'_e, p'_ω, p'_f

The relationships between the trajectory variables and orbit elements are well-known from celestial mechanics. One transformation from orbit elements to trajectory variables is

$$r = \frac{\alpha(1-e^2)}{1+e\cos f} \tag{A2}$$

$$\theta = \omega + f \tag{A3}$$

$$v = \sqrt{2(\xi + 1/r)} \tag{A4}$$

$$\gamma = \arctan\left(\frac{e\sin f}{1+e\cos f}\right). \tag{A5}$$

Similarly, one transformation from trajectory variables to orbit elements is

$$\xi = \frac{v^2}{2} - \frac{1}{r} \tag{A6}$$

$$\alpha = -1/(2\xi) \tag{A7}$$

$$p = (rv\cos\gamma)^2 \tag{A8}$$

$$e = (1 + 2\xi p)^{1/2} \tag{A9}$$

$$f = \arctan\left(\frac{p\tan\gamma}{p-r}\right) \tag{A10}$$

$$\omega = \theta - f. \tag{A11}$$

To transform the adjoint variables, the invariance of the Hamiltonian must be used. From eqn (A1)

$$p_r\,dr + p_\theta\,d\theta + p_v\,dv + p_\gamma\,d\gamma = p'_\alpha\,d\alpha + p'_e\,de + p'_\omega\,d\omega + p'_f\,df. \tag{A12}$$

Taking the differentials of the relationships between the trajectory variables and orbit elements in eqns (A2)–(A11) yields

$$d\omega = d\theta - df \tag{A13}$$

$$d\alpha = 2\alpha^2 v\,dv + \frac{2\alpha^2}{r^2}\,dr \tag{A14}$$

$$v\cos\gamma\,dr + r\cos\gamma\,dv - rv\sin\gamma\,d\gamma = \frac{1}{\sqrt{\alpha(1-e^2)}}[(1-e^2)\,d\alpha - 2\alpha e\,de] \tag{A15}$$

$$\frac{1}{\cos^2\gamma}\,d\gamma = \frac{\sin f}{(1+e\cos f)^2}\,de + \frac{e(e+\cos f)}{(1+e\cos f)^2}\,df. \tag{A16}$$

Combining these equations yields

$$de = \frac{(1-e^2)}{er}\left(\frac{\alpha}{r} - 1\right)dr + \frac{(1-e^2)}{e}\left(\alpha v - \frac{1}{v}\right)dv + \frac{rv\sqrt{\alpha(1-e^2)}}{\alpha e}\sin\gamma\,d\gamma \tag{A17}$$

$$e(e+\cos f)\,df = \alpha(1-e^2)v^2\,d\gamma - \sin f\,de. \tag{A18}$$

Substituting these into eqn (A12) gives

$$p\theta\,d\theta + p_r\,dr + p_v\,dv + p_\gamma\,d\gamma = p'_\omega\,d\theta + p'_\alpha\,d\alpha + \frac{(p'_f - p'_\omega)}{e(e+\cos f)}\alpha(1-e^2)v^2\,d\gamma + \left[p'_e - \frac{(p'_f - p'_\omega)\sin f}{e(e+\cos f)}\right]de. \tag{A19}$$

By expressing $d\alpha$ and de in terms of dr, dv, and $d\gamma$ and matching coefficients on the left-hand side, the desired canonical transformation between the two sets of adjoint variables is

$$p_r = \frac{2\alpha^2}{r^2}p'_\alpha + \left[p'_e - \frac{(p'_f - p'_\omega)\sin f}{e(e+\cos f)}\right]\frac{(e+\cos f)}{r} \tag{A20}$$

$$p_\theta = p'_\omega \tag{A21}$$

$$p_v = 2\alpha^2 v p'_\alpha + \left[p'_e - \frac{(p'_f - p'_\omega)\sin f}{e(e+\cos f)}\right]\frac{2(e+\cos f)}{v} \tag{A22}$$

$$p_\gamma = \frac{p'_e(1-e^2)\sin f}{(1+e\cos f)} + \frac{(p'_f - p'_\omega)}{e(1+e\cos f)}[e(1+e\cos f) + (e+\cos f)]. \tag{A23}$$

The relationships are linear in the adjoint and the coefficients are in mixed form but can easily be transformed into one or the other set of state variables.

Canonical Transformation Between Orbit Adjoint p'_α, p'_e, p'_ω, p'_f and Orbit Adjoint p_α, p_e, p_ω, p_M

The relationship between the two sets of orbit elements is quite simple. Introducing the eccentric anomaly E, the equations relating M and f are

$$M = E - e\sin E \tag{A24}$$

$$\tan\frac{f}{2} = \sqrt{\frac{1+e}{1-e}}\tan\frac{E}{2}. \tag{A25}$$

For a canonical transformation between the two sets of orbit elements, the Hamiltonian is invariant. Thus

$$p_\alpha\,d\alpha + p_e\,de + p_\omega\,d\omega + p_M\,dM = p'_\alpha\,d\alpha + p'_e\,de + p'_\omega\,d\omega + p'_f\,df \tag{A26}$$

Taking the differential of eqns (A24) and (A25) yields

$$dM = (1 - e\cos E)\,dE - \sin E\,de \tag{A27}$$

$$\tfrac{1}{2}\sec^2\frac{f}{2}\,df = \frac{1}{2}\sqrt{\frac{1+e}{1-e}}\sec^2\frac{E}{2}\,dE + \frac{\tan(E/2)}{(1-e)(1-e^2)^{1/2}}\,de. \tag{A28}$$

Solving eqn (A27) for dE gives

$$dE = \frac{1}{(1-e\cos E)}\,dM + \frac{\sin E}{(1-e\cos E)}\,de. \tag{A29}$$

Substituting dE into eqn (A28) yields

$$\tfrac{1}{2}\sec^2\frac{f}{2}df=\frac{1}{2}\sqrt{\frac{1+e}{1-e}}\sec^2\frac{E}{2}\left(\frac{dM}{(1-e\cos E)}+\frac{\sin E\,de}{(1-e\cos E)}\right)+\frac{1}{(1-e)(1-e^2)^{1/2}}\tan\frac{E}{2}de. \quad (A30)$$

To simplify the algebraic manipulations let

$$k_1=\frac{1}{2}\frac{(1+e)^{1/2}}{(1-e)^{1/2}(1-e\cos E)}\sec^2\frac{E}{2} \quad (A31)$$

$$k_2=k_1\sin E+\frac{1}{(1-e)(1-e^2)^{1/2}}\tan\frac{E}{2}. \quad (A32)$$

Solving eqn (A30) for df gives

$$df=2\cos^2\frac{f}{2}k_1\,dM+2\cos^2\frac{f}{2}k_2\,de. \quad (A33)$$

Substituting df into eqn (A26),

$$p_\alpha d\alpha+p_e de+p_\omega d\omega+p_M dM=p'_\alpha d\alpha+p'_e de+p'_\omega d\omega+p'_f\left(2\cos^2\frac{f}{2}k_1\,dM+2\cos^2\frac{f}{2}k_2\,de\right), \quad (A34)$$

and equating $d\alpha$, de, $d\omega$ and dM terms in eqn (A34) yields

$$p_\alpha=p'_\alpha \quad (A35)$$

$$p_e=p'_e+p'_f 2\cos^2\frac{f}{2}k_2 \quad (A36)$$

$$p_\omega=p'_\omega \quad (A37)$$

$$p_M=p'_f 2\cos^2\frac{f}{2}k_1. \quad (A38)$$

Substituting k_1 into eqn (A38) gives the following expression relating p_M and p'_f

$$p_M=p'_f\frac{\cos^2\frac{f}{2}(1+e)^{1/2}}{\cos^2\frac{E}{2}(1-e)^{1/2}(1-e\cos E)}.$$

Using eqn (A25) and some trigonometric identities, this simplifies to

$$p_M=p'_f\frac{\sin f}{\sin E(1-e\cos E)}. \quad (A39)$$

Substituting k_2 into eqn (A36) gives the following expression relating p_e, p'_e, and p'_f

$$p_e=p'_e+p'_f\left(\frac{\sin f}{1-e\cos E}+\frac{2\cos^2(f/2)\tan(E/2)}{(1-e)(1-e^2)^{1/2}}\right).$$

Using eqn (A25) and some trigonometric identities, p_e reduces to

$$p_e=p'_e+p'_f\left(\frac{\sin f}{1-e\cos E}+\frac{\sin f}{1-e^2}\right). \quad (A40)$$

Summarizing the results, the canonical transformation from p'_α, p'_e, p'_ω, p'_f to p_α, p_e, p_ω, p_M is

$$p_\alpha=p'_\alpha \quad (A41)$$

$$p_e=p'_e+p'_f\left(\frac{\sin f}{1-e\cos E}+\frac{\sin f}{1-e^2}\right) \quad (A42)$$

$$p_\omega=p'_\omega \quad (A43)$$

$$p_M=p'_f\frac{\sin f}{\sin E(1-e\cos E)}. \quad (A44)$$

This transformation can easily be inverted. Using the fact that

$$\frac{1-e\cos E}{1-e^2}=\frac{1}{1+e\cos f},$$

the canonical transformation from p_α, p_e, p_ω, p_M to p'_α, p'_e, p'_ω, p'_f is

$$p'_\alpha=p_\alpha \quad (A45)$$

$$p'_e=p_e-p_M\sin E\left(\frac{2+e\cos f}{1+e\cos f}\right) \quad (A46)$$

$$p'_\omega=p_\omega \quad (A47)$$

$$p'_f=p_M\frac{\sin E(1-e\cos E)}{\sin f}. \quad (A48)$$

Canonical Transformation Between Trajectory Adjoint p_r, p_θ, p_v, p_γ and Orbit Adjoint p_α, p_e, p_ω, p_M

Since the intermediate canonical transformations have already been developed, the canonical transformation between trajectory adjoint p_r, p_θ, p_v, p_γ and orbit adjoint p_α, p_e, p_ω, p_M is obtained by substituting eqns (A45)–(A48) into eqns (A20)–(A23)

$$p_r=\frac{2\alpha^2}{r^2}p_\alpha+\left[p'_e-\frac{(p'_f-p_\omega)\sin f}{e(e+\cos f)}\right]\frac{(e+\cos f)}{r} \quad (A49)$$

$$p_\theta=p_\omega \quad (A50)$$

$$p_v=2\alpha^2 v p_\alpha+\left[p'_e-\frac{(p'_f-p_\omega)\sin f}{e(e+\cos f)}\right]\frac{2(e+\cos f)}{v} \quad (A51)$$

$$p_\gamma=\frac{p'_e(1-e^2)\sin f}{(1+e\cos f)}+\frac{(p'_f-p_\omega)}{e(1+e\cos f)}\times[e(1+e\cos f)+(e\cos f)] \quad (A52)$$

$$p'_e=p_e-p_M\sin E\left(\frac{2+e\cos f}{1+e\cos f}\right) \quad (A53)$$

$$p'_f=p_M\frac{\sin E(1-e\cos E)}{\sin f}. \quad (A54)$$